Mapping densely packed GPIIb/IIIa receptors in murine blood platelets with expansion microscopy

Hannah S. Heil[1], Max Aigner[1], Sophia Maier[1], Prateek Gupta[1], Luise M.C. Evers[1], Vanessa Göb[1,2], Charly Kusch[1,2], Mara Meub[3], Bernhard Nieswandt[1,2], David Stegner[1,2*] and Katrin G. Heinze[1*]

[1] Rudolf Virchow Center for Integrative and Translational Bioimaging, University of Würzburg, Würzburg, Germany

[2] Institute of Experimental Biomedicine I, University Hospital Würzburg, Würzburg, Germany

[3] Department of Biotechnology and Biophysics, Biozentrum, University of Würzburg, Würzburg, Germany

* corresponding authors:

Katrin G. Heinze (katrin.heinze@virchow.uni-wuerzburg.de)

[1]Rudolf Virchow Center for Integrative and Translational Bioimaging, University of Würzburg, Würzburg, Germany

or David Stegner (stegner@virchow.uni-wuerzburg.de)

[2]Institute of Experimental Biomedicine, University Hospital Würzburg, Würzburg, Germany
`

Running title: Mapping platelet receptors with ExM

Abstract

Interrogating small platelets and their densely packed, highly abundant receptor landscape is key to understand platelet clotting, a process that can save lives when stopping blood loss after an injury, but also kill when causing heart attack, stroke or pulmonary embolism. The underlying key receptor distributions and interactions, in particular the relevance of integrin clustering, are not fully understood is because of highly abundant and densely distributed GPIIb/IIIa receptors. This makes receptor distributions difficult to assess even by super-resolution fluorescence microscopy. Here, we combine dual-color expansion and confocal microscopy with colocalization analysis to assess platelet receptor organization without the need of a super-resolution microscope. We show that 4x expansion is highly straight-forward for super-resolution microscopy of platelets, while 10x expansion provides higher precision at the price of increased efforts in sample preparation and imaging. Quantifying various receptor colocalization scenarios we demonstrate that expansion microscopy can pinpoint receptor distributions and interactions in resting and activated platelets being superior to conventional methods that fail in such dense 3D scenarios with highly abundant receptors. We reveal the presence of GPIIb/IIIa clusters in resting platelets, which are not affected by platelet activation indicating that they contribute to the rapid platelet response during platelet clotting.

Graphical Abstract

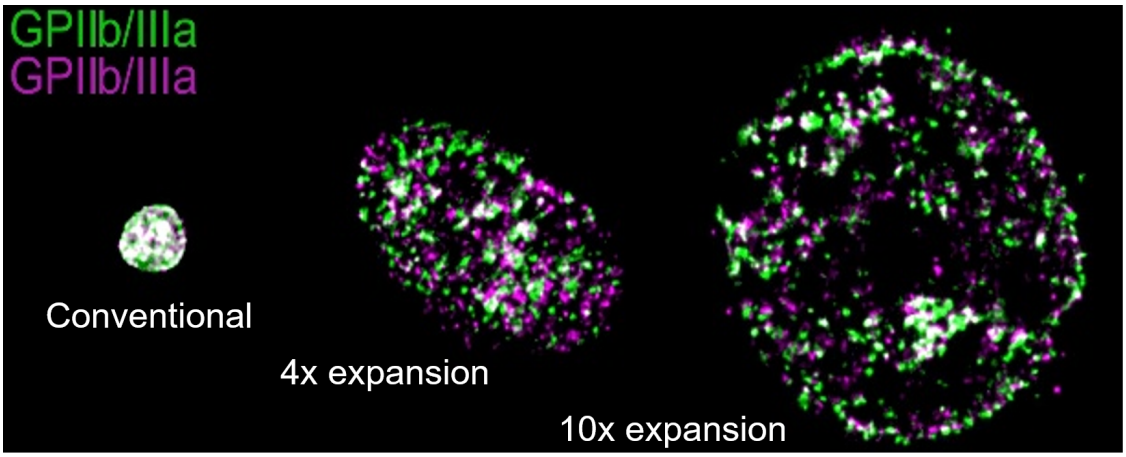

Keywords: Integrin, blood platelets, receptor mapping, super-resolution microscopy, colocalization

Introduction

Integrins are a superfamily of heterodimeric cell-surface receptors that comprise an α and a β subunit.[1,2] Each subunit consist of a large N-terminal extracellular domain that contributes to ligand binding, a single-pass transmembrane domain and a cytoplasmic tail providing binding sites for adaptors, and signaling proteins that contribute to the bidirectional integrin signaling.[3,4] Integrin receptors are widely expressed in mammalian tissues and serve as adhesive units, which are, however, highly dynamic regulators of cellular responses. This is in particular true for platelets that require an acute and dynamic regulation of integrin affinity and ligand binding to enable rapid platelet adhesion at sites of vascular injury on the one hand and to prevent uncontrolled thrombosis of the other hand. The αIIbβ3 integrin (also named GPIIb/IIIa or CD41/CD61) is exclusively expressed by megakaryocytes and platelets and binds a number of ligands, including fibrinogen, fibrin, fibronectin and von Willebrand factor.[5] This receptor is of high clinical relevance as GPIIb/IIIa inhibitors are widely used to prevent thrombosis and treat myocardial infarction.[6] Moreover, GPIIb/IIIa serves as model receptor to study integrin biology.[4] In the last decades key components of both inside-out and outside-in signaling have been identified; the first represents the functional up-regulation of the receptor's affinity, the latter generates integrin-mediated signaling responses following ligand binding.[3,4] In addition, it is widely accepted that clustering of integrin receptors in hetero-oligomers modulates avidity and supports the assembly of the outside-in signalosome;[7,8] unfortunately, our current understanding of the underlying processes and the receptor distribution is far from complete.[4,9] One reason is the high receptor density on the platelet surface. Platelets are small in size (2-3 µm in diameter) and express 50,000-100,000 copies of GPIIb/IIIa on their surface, while even more can be mobilized from intracellular stores.[10,11] Thus, visualizing and quantifying GPIIb/IIIa distribution on the platelet surface is very challenging. Strictly spoken, a resolution in the nanometer range is required to gain an image based receptor map on the single molecule level.[12] Electron microscopy would provide such nanometer resolution, however, despite its unrivaled resolution power, it lacks efficient staining for specific receptors and immunogold labeling is hard to achieve at saturating conditions. In contrast, fluorescence labeling is efficient and selective and thus allows visualization of single membrane receptors when combined with super-resolution imaging.[13–15] A variety of fluorescence super-resolution modalities have been reported over the past century, each with its own advantages and limitations.[16] Multi-color

3D single molecule localization microscopy allows to effectively decipher receptor interaction and organization at a molecular level; however, it requires a high level of expertise and equipment and fails at high molecular density scenarios[17] such as highly abundant and dense platelet receptor distributions we are tackling here. A particularly promising, rather young method is expansion microscopy (ExM).[18] In contrast to most other super-resolution techniques ExM does not require a high-end super-resolution microscope but uses physical volumetric expansion of the sample. Linking the fluorescently labeled proteins to a swell-able hydrogel eventually turns any conventional microscope into a super-resolution imaging device. The major downside is that isotropic expansion requires a highly processed sample and harsh preparation steps: After fixation and immunolabeling the sample structure itself needs to be tightly linked into the hydrogel network and has to be disrupted by breaking protein bonds and crosslinks through either protein digestion or degradation[19]. Depending on the hydrogel composition the gel will swell up to 10x of its original size expanding the sample to up to 1000x of its original volume[20] (see also supplemental Figure I). With physical expansion, the labeling density decreases respectively, and the sample additionally undergoes harsh chemical treatment during gelation and digestion, which typically results in a 50% loss of fluorescent markers.[19] Nevertheless, the resolution gain by ExM allows quantitative image-based comparison of two (fluorescently labeled) molecular distributions. Eventually, a colocalization coefficient can be calculated providing an intensity correlation measure of both color channels.[21] The commonly used Pearson's colocalization coefficient excels in robustness under varying signal-to-noise conditions, however fails when number of events detected in each channel are not comparable. The two Manders' colocalization coefficients are less robust to noise, but make analysis more versatile as the approach allows to directly retrieve the overlapping fraction of one protein to the other and vice versa.[22] In ExM reporting the overlapping fraction regardless of the degree of asymmetric signal loss in both channels is crucial.

Here we show how ExM and image analysis can be tuned to advance studies of dense and highly abundant platelet receptor interactions, which are difficult to tackle otherwise. Our quantitative approach involves a combination of ExM, confocal microscopy and colocalization analysis with optimized sample preparation for 4x and 10x expansion as well as tailored image analysis pipelines. Supported by a simulation tool for platelet receptor distributions we find that only 10x expansion provides the required resolution to

88 distinguish colocalized from independent receptor distributions for highly abundant
89 GPIIb/IIIa and GPIX receptors on resting and activated platelets.

90 Methods

91 The authors declare that materials and data are available upon reasonable request from
92 the authors. A selection of typical images and the code for simulation of platelet receptor
93 distributions are available on ZENODO (doi: 10.5281/zenodo.4117555), where we also
94 provide a video protocol of the sample preparation for 10x ExM. An extended version of
95 Materials and Methods as well as detailed supplementary protocols for 4x and 10x platelet
96 ExM are available in the Supplemental Material. All methods were carried out in
97 accordance with relevant guidelines and regulations.

98 Platelet Isolation

99 C57Bl/6J mice served as blood donors and animal experiments were approved by the
100 district government of Lower Franconia (Bezirksregierung Unterfranken). Washed
101 platelets were prepared as described elsewhere[23]. Round coverslips (Ø12 mm, #1.5 , #1.5
102 Menzel and Ø24 mm, #1.5 Plano GmbH) were cleaned by 1 h sonication in chloroform
103 (472476, Sigma), followed by 1 h sonication in NaOH (6771, Roth), ddH_2O washed, dried
104 at 70°C and stored in Ethanol (34852, Sigma). The clean coverslips were coated with 2 M
105 glycine (A1067, AppliChem) in PBS for 10 min and washed 2x with PBS and 1x with
106 Tyrodes buffer. The platelet suspension was deposited onto the coated coverslips ($30*10^6$
107 / $15*10^6$ platelets for 24 mm/12 mm) and incubated for 30 min at 37°C for settling. Platelet
108 activation was achieved by complementing the Tyrodes buffer with 2 mM Ca^{2+} and the
109 addition of 0.01 U/ml Thrombin (10602400001, Roche) to the platelet suspension.

110 Immunostaining

111 *Fixation:* Platelets were fixed with glyoxal solution (19.89% (wt/wt) pure ethanol, 3.15%
112 (wt/wt) glyoxal (128465, Sigma), 0.7% (wt/wt) acetic acid (7332.1, Roth) in ddH_2O) at pH
113 5.0 for 20 min [24] at RT, washed 5x with PBS and blocked with 5% bovine serum albumin
114 (BSA, A3983, Sigma) in PBS for 2 h, then washed with PBS.

115 *Immunolabeling*: Platelets were immersed in 10 µg/ml fluorescently labeled antibody
116 (produced in-house: IgG MWReg30 against GPIIb/IIIa, IgG JON6 against GPIIb/IIIa on
117 different epitope, and IgG p0p6 against GPIX as described previously[25]) conjugated with

118 Alexa Fluor 488 (A20181, Thermo Fisher) or Alexa Fluor 594 (A20185, Thermo Fisher)
119 solved in PBS with 5% BSA for 30 min at 37°C, ensuring saturated labeling of all available
120 epitopes (tested with flow cytometry). Afterwards, coverslips were washed 5x with PBS.
121 The antibodies' degree of labelling was measured by spectrometric analysis (NanoDrop
122 One, Thermo Fisher Scientific).

123 **Platelet Expansion**

124 *4x expansion* (adapted from Chozinski et al 2016 [26]). Immunolabeled platelets on
125 coverslips were incubated at RT with linking solution (0.1 mg/ml Acryloyl-X in PBS,
126 A20770, Invitrogen) for 12 h. A 50 µl drop of monomer solution (2 M NaCl, 2.5% (wt/wt)
127 acrylamide (AA, A9099, Sigma), 0.15% (wt/wt) N,N′-methylenebisacrylamide (M7279,
128 Sigma), 8.625% (wt/wt) sodium acrylate (SA, 408220, Sigma) in PBS), containing 0.2%
129 freshly added ammonium persulfate (APS, 9592.3, Roth) and tetramethylethylenediamine
130 (TEMED, 2367.3, Roth) was placed on elastic film (parafilm, Sigma) and covered by the
131 sample glass coverslip (2x washed with PBS). After gelation for 2 h at RT in a humidified
132 chamber the samples were transferred into digestion buffer (8 U/ml Proteinase K (P4850,
133 Sigma), 50 mM Tris pH 8.0, 1 mM EDTA (ED2P, Sigma), 0.5% Triton X-100 (28314,
134 Thermo Fisher) and 0.8 M guanidine HCl (50933, Sigma) in ddH_2O), and incubated
135 overnight (8 h) in a humidified chamber. After removal of the coverslip the gel was
136 expanded in ddH_2O for 24 hours, immobilized on a poly-D-lysine (02102694, MP
137 Biomedicals) coated Ø24 mm, #1.5 coverslip and imaged.

138 *10x expansion* (adapted from Truckenbrodt *et al*. 2018 [27] and modified). The 10x monomer
139 solution consists of 2.67% (wt/wt) N,N-dimethylacrylamide (DMAA, 274135, Sigma), and
140 0.64% (wt/wt) sodium acrylate (SA) in ddH_2O and was bubbled with N_2 to purge out
141 molecular oxygen for 40 min on ice before adding 0.0036 g/ml of KPS (206224, Sigma).
142 After another 15 min of O_2 purging 0.4% TEMED were added, and 50 µl of final monomer
143 solution immediately placed on elastic film and covered with the sample (on coverslip).
144 After gelation in a N_2-filled humidified chamber for 48 h at 4°C, digestion was performed
145 for 12 h at 50°C.

146 **Fluorescence Imaging**

147 Dual color confocal microscopy was used (Leica TCS SP5 II; 63x 1.2 NA water immersion
148 objective, 8000 Hz resonant scanning; pixels: 1024x1024, voxels: x,y = 41 nm & z=170

149 nm, pinhole: 1 Airy unit, scanning: 8x line averaging, 3 frames accumulated, exc.: 488 nm
150 & 561 nm, detection: 500-550 and 600-650 nm in sequential mode, Hybrid detector (HyD).
151 Chromatic aberrations were corrected by distortion matrices using bUnwarpJ[28] (calibration
152 by 100 nm 4-colour fluorescent microspheres (TetraSpeck, T7279) as described
153 elsewhere[29]). Images were deconvolved (Huygens Professional, SVI, Leiden,
154 Netherlands) with a theoretical PSF and a signal-to-noise threshold of 30 counts.

155 **Data Analysis**

156 Image preprocessing, colocalization analysis and statistical validation, as well as the
157 simulation, dSTORM imaging and analysis are described in detail in the *Online*
158 *Supplementary Methods*.

159

160 Results

161 **Optimizing ExM for receptor colocalization on platelets**

162 The accuracy of a colocalization study mainly depends on the spatial resolution of the
163 underlying image.[12] In order to compare the performance of the colocalization analysis for
164 different resolution levels, we established two different kinds of expansion protocols
165 leading to 4x and 10x expansion along previously published work.[19,27] Before
166 immunolabeling and expansion, purified resting platelets are settled on a glycine coated
167 surface and chemically fixed without any signal compromise (supplemental Figure II A,B)
168 to avoid unintended receptor reorganization by platelet activation. Here, glyoxal fixation
169 outperformed PFA fixation in both, labeling efficiency and minimal background signal[24]
170 (supplemental Figure II C,D).

171 Figure 1A shows the respective deconvolved confocal images of GPIIb/IIIa receptors on
172 unexpanded versus 4x and 10x expanded platelets. The GPIIb/IIIa receptors are targeted
173 by monoclonal antibodies carrying *either* an Alexa Fluor 594 (Figure 1, magenta) *or* an
174 Alexa Fluor 488 marker (Figure 1, green). Thus, this assay is designed to show low
175 colocalization if resolution is sufficient and clustering is low. For unexpanded small
176 platelets, however, low image resolution leads to a linear relationship in the intensity
177 scatter plot for the two color channels (Figure 1B). Such largely overlapping color signals
178 only provide a meaningless high degree of – potentially false-positive – co-localization. In

179 contrast, with 4x and 10x expanded platelets this linear relationship vanishes and
180 colocalization analysis becomes discernible for different scenarios (Figure 1 C, D).
181 Unfortunately, the resolution gain is accompanied by a loss in contrast due to reduced
182 signal-to-noise ratio (Figure 1E). Moreover, the signal retention varies for different
183 fluorescent dyes. While both antibodies were decorated with a similar number of
184 fluorophores (see supplemental Table I), the signal retention is different for each color
185 (Figure 1F, lower signal retention in the green channel than in the magenta channel). Low
186 contrast and different degree of receptor visibility between channels require a careful
187 preselection of the colocalization modality.

188 The Manders' colocalization approach turned out to be the only applicable here as it is
189 most crucial that the channel with fewer events still reports its overlapping fraction
190 regardless of the degree of asymmetric signal loss in both channels. As the Manders'
191 colocalization coefficient, however, is less robust against noise than the commonly used
192 Pearson's colocalization coefficient, image preprocessing is required to exclude
193 background signal efficiently.[13] Along these requirements, we compiled an image
194 processing pipeline providing a chromatic shift correction (Figure 2A) before a
195 deconvolution step (Figure 2B) followed by background filtering (Figure 2 C,D). In the last
196 step signal events are filtered by intensity threshold and size (detailed description in the
197 supplementary methods).

198 **Receptor distributions revealed by expansion of platelets**

199 ExM increases the optical resolution level to the nanometer range; the exact resolution
200 gain depends on the hydrogel composition and the respective expansion factor. This
201 means that in principle a lateral resolution of down to 25 nm can be realized by 10x
202 expansion and confocal microscopy; however, as this resolution gain comes at the
203 expense of image brightness and contrast, we carefully dissected the resolution level that
204 is required for colocalization analysis of the platelet receptors. First, we used realistic
205 simulations (see Figure 3 and 4) to understand how the image quality and specificity would
206 manifest itself under real experimental conditions. Therefore, randomly distributed single
207 GPIIb/IIIa receptors or receptor clusters as fluorescent objects were computationally
208 placed on a spheroid surface reflecting typical mouse platelet dimensions (Figure 3). From
209 such platelet-like objects (Figure 3A) fluorescence images (Figure 3B-D representing
210 maximal (left) and minimal (right) colocalization) were created including realistic

211 background signal and noise (unexpanded: Figure 3B, 4x expanded: Figure 3C, 10x
212 expanded: Figure 3D). The resulting signal-to-noise ratios of these simulated 3D images
213 for all three expansion levels (none, 4x, 10x) and the two colocalization cases in
214 comparison are plotted in dependence of increasing marker retention ratio. Even if the
215 signal-to-noise level is higher for lower expansion factors, the colocalization coefficient
216 becomes meaningless when looking at platelet receptor distributions with varying
217 densities (Figure 4A) for a high and low colocalization test case (Figure 4B). For the high
218 colocalization case, two markers can bind to one individual receptor at the same time
219 giving rise to a high colocalization coefficient, while in the low colocalization case the two
220 markers have less chance to colocalize as each receptor can only by occupied by either
221 one marker (Figure 4B). In unexpanded platelets it is impossible to distinguish both cases
222 reliably while this was possible for expanded platelets in the whole receptor density range.
223 For a receptor density in the range ~500 /µm² as we found for GPIIb/IIIa (see supplemental
224 Figure III) 4x expansion is expected to only show a 10% drop in colocalization between
225 the high and low case, while at 10x expansion a drop of 50% can be expected (Figure
226 4A). Thus, only 10x expansion provides sufficient dynamic range to pinpoint the
227 differences of receptor colocalization in the two test cases. This advantage vanishes only
228 if marker retention would drop below 50% (Figure 4C). Note that for both, 4x and 10x
229 expansion, the achieved super-resolution is just not sufficient to resolve single molecules
230 and thus may still leave a certain risk to detect "false-positive" colocalizations. Here in this
231 case, even for very low receptor densities a Manders' colocalization coefficient of 0.6 or
232 0.2, respectively, represents the low colocalization case. To understand how the loss of
233 markers during homogenization and expansion influence these results, we additionally
234 accounted for the clustered arrangement of GPIIb/IIIa on resting platelets as observed by
235 single molecule localization microscopy (Figure 4D & supplemental Figure III). Decreasing
236 marker retention in both channels means smaller colocalization values (Figure 4E),
237 particularly in 4x expansion where the dynamic range between high and low colocalization
238 is decreased for retention ratios below 50%; in contrast, for 10x expansion the
239 performance is best maintained even beyond 50%. However, with further decreasing
240 (asymmetric) retention ratio the analysis becomes prone to artifacts (Figure 3 &
241 Figure 4F): When the retention ratio is fixed at 60% in channel A and the retention ratio of
242 channel B ranges from 100% to 20% the results seem to be robust down to only 40%
243 retention in channel B for both 4x and 10x expansion. In 4x expansion the dynamic range
244 between the high and low colocalization are indistinguishable (high and low, Figure 4B) at

245 20% retention in channel B. The high colocalization is experimentally realized with two
246 antibodies carrying either dye molecule or targeting different epitopes on GPIIb/IIIa. Thus,
247 they can bind to a single receptor at the same time (supplemental Figure IV*, case I).*

248 Next, we would like to look at true experimental data. For image preprocessing and
249 analysis, it is important to include only platelets above the largest cutoff and with suitable
250 orientations to avoid bias in the subsequent colocalization analysis (Figure 5). Thus, we
251 excluded not fully expanded platelets from further analysis (Figure 5A), and made sure
252 that subpopulations of platelets with different orientations are correctly reflected in the
253 distribution of Manders' colocalization coefficients (Figure 5 B,C). Now, we are fully
254 prepared to interrogate three different colocalization scenarios: For the high colocalization
255 case two antibodies targeting two different epitopes of GPIIb/IIIa are used carrying Alexa
256 Fluor 488 and Alexa Fluor 594 respectively (Figure 6, case I). For the low colocalization,
257 only one antibody targeting a single epitope of GPIIb/IIIa is used, carrying either Alexa
258 Fluor 488 or Alexa Fluor 594 (Figure 6A, case II). As an additional case (case III, Figure
259 6) we introduce two independent receptors, GPIIb/IIIa and GPIX, which are targeted with
260 distinct fluorophores and no colocalization is expected.

261 For unexpanded platelets (Figure 6A left) high Manders' colocalization coefficients are
262 observed for all three test cases and differences in the marker arrangement are not
263 resolved (Figure 6B). In line with previous reports by others[30] our results here underscore
264 that conventional confocal microscopy completely fails when it comes colocalization
265 studies of densely packed targets. By expanding the platelets 4x the coefficient for case I
266 drops down to ~0.6 due to the limited retention ratio. It can already be distinguished from
267 case III with a dynamic range of 0.15 between maximum and minimum colocalization while
268 the resolution is insufficient to distinguish it from case II. The increase in resolution
269 achieved with 10x expansion allows to extend the dynamic range of the Manders'
270 colocalization coefficient to 0.25. While in the 4x expansion experiments the limited
271 resolution still leads to an apparent Manders' colocalization coefficient of ~0.5 for case II
272 and III, it drops down to ~30% for 10x expansion with a clear separation between the high
273 and low colocalization. Simulated data shows 4x expansion does not provide the
274 resolution required at the given receptor densities. Interestingly, case II yields a higher,
275 but not significantly different colocalization coefficient than case III, maybe due to the
276 higher abundance of the GPIIb/IIIa receptors. Fortunately, a neighbor-distance analysis of

277 10x expanded platelets allows to distinguish colocalized, clustered and non-interacting
278 receptor distributions (supplemental Figure V) overcoming its lack of molecular resolution.

279 In an independent experiment we compared the GPIIb/IIIa distribution on resting and
280 activated platelets to assess whether platelet activation affects the formation of integrin
281 clusters. Surprisingly, GPIIb/IIIa colocalization coefficients of activated platelets were
282 comparable to those in resting platelets (Figure 6C,D), suggesting that the organization of
283 GPIIb/IIIa receptors is conserved during platelet activation.

284

285 **Discussion**

286 This study shows that the combination of ExM and confocal imaging is a powerful tool to
287 study platelet receptor organization and interaction in small blood platelets and dense and
288 highly abundant receptor scenarios where other high- and super-resolution methods fail.
289 Conventional confocal microscopy alone is not suited as demonstrated here. Based on an
290 optimized sample preparation and tailored image preprocessing and analysis procedure
291 we developed a colocalization analysis approach which allows to classify the distribution
292 and interaction of high-density platelet receptor populations. Our findings suggest, that
293 GPIIb/IIIa receptors are present in pre-formed clusters already on resting blood platelets.
294 These pre-formed clusters might play a role in enhancing platelet adhesion and
295 aggregation following inside-out activation and thereby contribute to the rapid platelet
296 responses upon vascular injury. The unexpected observation that these clusters are not
297 affected by platelet activation (Figure 6D) supports this hypothesis. These data indicate
298 that – at least in the absence of an immobilized ligand – no significant rearrangement of
299 GPIIb/IIIa clusters relative to each other is observed. One might speculate that these
300 uniformly distributed clusters represent preassembled outside-in signalosomes that are
301 'ready to go' upon integrin-ligand binding or inside-out signaling. Thereby, they enable
302 ligand binding on the entire platelet surface, allowing a rapid response to external stimuli.
303 Clearly, further studies are needed to elucidate the receptor interplay on the platelet
304 surface. In particular, the effects of immobilized ligands on the distribution of GPIIb/IIIa
305 clusters are worth studying, to investigate whether such ligands would result in bigger
306 GPIIb/IIIa clusters along the ligands similar to GPVI.[31,32]On the other hand it is also
307 possible that these uniformly GPIIb/IIIa clusters are critical for the mechanosensing
308 capacity of platelets and potentially platelet migration.[33,34]

In any case our study successfully addresses the special requirements posed by the small platelet size and high receptor density. While alternative super-resolution microscopy techniques can provide single molecule resolution, which is not achieved here, the presented approach stands out by its accessibility as it does not require an advanced super-resolution setup. Furthermore, the combination with confocal microscopy allows for the implementation of both, 3D and multicolor imaging, still bottlenecks for many super-resolution techniques.

However, regarding colocalization analysis the approach itself holds intrinsic challenges as it not only lacks the mentioned single molecule sensitivity, but also suffers from a significant loss of fluorescent markers. We evaluated the performance of ExM based colocalization analysis regarding receptor density and retention ratios based on simulated GPIIb/IIIa receptor distributions. While an expansion of 4x still provides robust results at retention ratios below 50%, the dynamic range between high and low colocalization is significantly lower than for 10x expansion and especially for receptor densities above 1000/µm² only 10x expansion provides sufficient resolution to distinguish both cases. As mentioned before, the marker retention ratio greatly depends on the sample processing as well as the molecular properties of the fluorescent dye. For the organic dyes Alexa Fluor 488 and Alexa Fluor 594 used in this study, retention ratios of ~50% have been reported.[19]

The higher resolution achieved by 10x expansion comes at the cost of signal dilution, a longer and harsher sample preparation and a decreased mechanical stability of the hydrogel. To address the issue of signal loss and dilution, several modifications of the anchoring chemistry and homogenization procedure have been reported to allow post expansion labeling.[35–37]

Despite these limitations ExM will help to improve our understanding of platelet receptor distribution. This will have implications on our understanding of platelet integrin receptor stoichiometry and spatial organization like in the present study. We have established ExM for murine platelets as this allows to combine this attractive technology with transgenic models to investigate further research questions in the platelet field, like the existence/relevance of clusters of (hem)ITAM receptors,[38,39] lipid rafts[40] or the question whether different pools of α-granules exist in platelets.[41,42] By combining ExM with advanced imaging techniques it is even possible to achieve molecular resolution[37,43–45] if

the marker and labeling concept allows. Thus, we believe that ExM for platelet imaging has a bright future and may soon help to decipher complex receptor interactions within the nanometer range.

Acknowledgments

K.G.H., D.S., B.N. and H.S.H conceived and designed the experiments. H.S.H. performed the simulations for the resting platelets and supervised the ExM experiments. M.A. developed the platelet expansion protocol and the image acquisition procedure and developed the image processing and colocalization analysis procedures. M.A. and S.M. performed the ExM experiments and analysis on resting platelets. P.G. performed the ExM experiments on activated platelets while L.M.C.E. performed the data analysis. C.K. and M.M. performed the dSTORM imaging and cluster analysis. P.G. and S.M. performed the confocal imaging on activated and resting platelets respectively. V.G. screened the antibody incubation times for live and post-fix labelling and assisted with the animal handling. D.S., B.N. and V.G. advised with the platelet preparation and immunolabeling. B.N. provided the platelet antibodies. K.G.H., H.S.H and D.S. wrote the paper. All authors read and approved the final manuscript. We thank Shazeb Ahmad and Christoph Kempe for assistance in protocol development of ExM, Dr. Katharina Remer for support with documentation and management of animal experimentation and welfare, as well as Harald Schulze and Markus Sauer for fruitful discussion around platelet biology, expansion microscopy and colocalization analysis. Thanks to A. Balakrishnan for proof-reading.

Source of Funding

This study was supported by the Deutsche Forschungsgemeinschaft (SFB/TR 240, project number 374031971, B06 to D.S.; individual project HE 6438/4-1 to K.G.H. and NI 556/13-1 to B.N.), the Medical Faculty and the Graduate School of Life Sciences GSLS of the University of Würzburg (doctoral stipend to M.A. and S.M.), and the Rudolf-Virchow-Center of the University of Würzburg (H.S.H.).

370 **Disclosures**

371 DS is on the editorial board of *Platelets*. All other authors have no conflicts of interest.

372

373 **References**

374 1. Hynes, R. O. Integrins: Bidirectional, Allosteric Signaling Machines. *Cell* **110**,
375 673–687 (2002).

376 2. Campbell, I. D. & Humphries, M. J. Integrin Structure, Activation, and Interactions.
377 *Cold Spring Harb. Perspect. Biol.* **3**, a004994–a004994 (2011).

378 3. Shattil, S. J., Kim, C. & Ginsberg, M. H. The final steps of integrin activation: the
379 end game. *Nat. Rev. Mol. Cell Biol.* **11**, 288–300 (2010).

380 4. Durrant, T. N., van den Bosch, M. T. & Hers, I. Integrin αIIbβ3 outside-in signaling.
381 *Blood* **130**, 1607–1619 (2017).

382 5. Humphries, J. D. Integrin ligands at a glance. *J. Cell Sci.* **119**, 3901–3903 (2006).

383 6. Mackman, N., Bergmeier, W., Stouffer, G. A. & Weitz, J. I. Therapeutic strategies
384 for thrombosis: new targets and approaches. *Nat. Rev. Drug Discov.* **19**, 333–352
385 (2020).

386 7. Fong, K. P. *et al.* Directly Activating the Integrin αIIbβ3 Initiates Outside-In
387 Signaling by Causing αIIbβ3 Clustering. *J. Biol. Chem.* **291**, 11706–11716 (2016).

388 8. Legate, K. R., Wickstrom, S. A. & Fassler, R. Genetic and cell biological analysis
389 of integrin outside-in signaling. *Genes Dev.* **23**, 397–418 (2009).

390 9. Huang, J. *et al.* Platelet integrin αIIbβ3: signal transduction, regulation, and its
391 therapeutic targeting. *J. Hematol. Oncol.* **12**, 26 (2019).

392 10. Wagner, C. *et al.* Analysis of GPIIb/IIIa receptor number by quantification of 7E3
393 binding to human platelets. *Blood* **88**, 907–914 (1996).

394 11. Coller, B. S. & Shattil, S. J. The GPIIb/IIIa (integrin αIIbβ3) odyssey: a technology-
395 driven saga of a receptor with twists, turns, and even a bend. *Blood* **112**, 3011–
396 3025 (2008).

397 12. Oheim, M. & Li, D. Quantitative Colocalisation Imaging: Concepts, Measurements,
398 and Pitfalls. in *Imaging Cellular and Molecular Biological Functions* (eds. Shorte,
399 S. L. & Frischknecht, F.) 117–155 (Springer Berlin Heidelberg, 2007).
400 doi:10.1007/978-3-540-71331-9_5.

401 13. Pike, J. A., Styles, I. B., Rappoport, J. Z. & Heath, J. K. Quantifying receptor
402 trafficking and colocalization with confocal microscopy. *Methods* **115**, 42–54
403 (2017).

404 14. Schulze, H. & Stegner, D. Imaging platelet biogenesis in vivo. *Res. Pract.*
405 *Thromb. Haemost.* **2**, 461–468 (2018).

406 15. Clark, J. C. *et al.* Adenosine and Forskolin Inhibit Platelet Aggregation by
407 Collagen but not the Proximal Signalling Events. *Thromb. Haemost.* **119**, 1124–
408 1137 (2019).

409 16. Vangindertael, J. *et al.* An introduction to optical super-resolution microscopy for
410 the adventurous biologist. *Methods Appl. Fluoresc.* **6**, 022003 (2018).

411 17. Levet, F. *et al.* A tessellation-based colocalization analysis approach for single-
412 molecule localization microscopy. *Nat. Commun.* **10**, 1–12 (2019).

413 18. Chen, F., Tillberg, P. W. & Boyden, E. S. Expansion microscopy. *Science* **347**,
414 543–548 (2015).

415 19. Tillberg, P. W. *et al.* Protein-retention expansion microscopy of cells and tissues
416 labeled using standard fluorescent proteins and antibodies. *Nat. Biotechnol.* **34**,
417 987–992 (2016).

418 20. Truckenbrodt, S., Sommer, C., Rizzoli, S. O. & Danzl, J. G. A practical guide to
419 optimization in X10 expansion microscopy. *Nat. Protoc.* **14**, 832–863 (2019).

420 21. Dunn, K. W., Kamocka, M. M. & McDonald, J. H. A practical guide to evaluating
421 colocalization in biological microscopy. *Am. J. Physiol. Physiol.* **300**, C723–C742
422 (2011).

423 22. Manders, E. M. M., Verbeek, F. J. & Aten, J. A. Measurement of co-localization of
424 objects in dual-colour confocal images. *J. Microsc.* **169**, 375–382 (1993).

425 23. van Eeuwijk, J. M. M. *et al.* The Novel Oral Syk Inhibitor, BI1002494, Protects
426 Mice From Arterial Thrombosis and Thromboinflammatory Brain Infarction.
427 *Arterioscler. Thromb. Vasc. Biol.* **36**, 1247–1253 (2016).

428 24. Richter, K. N. *et al.* Glyoxal as an alternative fixative to formaldehyde in
429 immunostaining and super-resolution microscopy. *EMBO J.* **37**, 139–159 (2018).

430 25. Nieswandt, B., Bergmeier, W., Rackebrandt, K., Gessner, J. E. & Zirngibl, H.
431 Identification of critical antigen-specific mechanisms in the development of
432 immune thrombocytopenic purpura in mice. *Blood* **96**, 2520–2527 (2000).

433 26. Chozinski, T. J. *et al.* Expansion microscopy with conventional antibodies and
434 fluorescent proteins. *Nat. Methods* **13**, 485–488 (2016).

435 27. Truckenbrodt, S. *et al.* X10 expansion microscopy enables 25-nm resolution on
436 conventional microscopes. *EMBO Rep.* **19**, e45836 (2018).

437 28. Arganda-Carreras, I. *et al.* Consistent and Elastic Registration of Histological
438 Sections Using Vector-Spline Regularization. in *Computer Vision Approaches to*
439 *Medical Image Analysis* 85–95 (2006). doi:10.1007/11889762_8.

440 29. Heil, H. S. *et al.* Sharpening emitter localization in front of a tuned mirror. *Light*
441 *Sci. Appl.* **7**, 99 (2018).

442 30. Brunstein, M. & Oheim, M. Dependence of descriptors of co-localization on
443 microscope spatiotemporal resolution and the choice of regions of interest.
444 *Microsc. Res. Tech.* **80**, 220–230 (2017).

445 31. Poulter, N. S. *et al.* Clustering of glycoprotein VI (GPVI) dimers upon adhesion to
446 collagen as a mechanism to regulate GPVI signaling in platelets. *J. Thromb.*
447 *Haemost.* **15**, 549–564 (2017).

448 32. Pallini, C. *et al.* Immobilized collagen prevents shedding and induces sustained
449 GPVI clustering and signaling in platelets. *Platelets* **32**, 59–73 (2021).

450 33. Gaertner, F. *et al.* Migrating Platelets Are Mechano-scavengers that Collect and
451 Bundle Bacteria. *Cell* **171**, 1368-1382.e23 (2017).

452 34. Nicolai, L. *et al.* Vascular surveillance by haptotactic blood platelets in
453 inflammation and infection. *Nat. Commun.* **11**, 5778 (2020).

454 35. Ku, T. *et al.* Multiplexed and scalable super-resolution imaging of three-
455 dimensional protein localization in size-adjustable tissues. *Nat. Biotechnol.* **34**,
456 973–981 (2016).

457 36. Gambarotto, D. *et al.* Imaging cellular ultrastructures using expansion microscopy
458 (U-ExM). *Nat. Methods* **16**, 71–74 (2019).

459 37. Zwettler, F. U. *et al.* Molecular resolution imaging by post-labeling expansion
460 single-molecule localization microscopy (Ex-SMLM). *Nat. Commun.* **11**, 3388
461 (2020).

462 38. Rayes, J., Watson, S. P. & Nieswandt, B. Functional significance of the platelet
463 immune receptors GPVI and CLEC-2. *J. Clin. Invest.* **129**, 12–23 (2019).

464 39. Senis, Y. A., Mazharian, A. & Mori, J. Src family kinases: at the forefront of
465 platelet activation. *Blood* **124**, 2013–2024 (2014).

466 40. Lee, F. A. *et al.* Lipid rafts facilitate the interaction of PECAM-1 with the
467 glycoprotein VI-FcR γ-chain complex in human platelets. *J. Biol. Chem.* **281**,
468 39330–39338 (2006).

469 41. Battinelli, E. M. *et al.* Megakaryocytes package contents into separate a-granules
470 that are differentially distributed in platelets. *Blood Adv.* **3**, 3092–3098 (2019).

471 42. Yadav, S. & Storrie, B. The cellular basis of platelet secretion: Emerging
472 structure/function relationships. *Platelets* **28**, 108–118 (2017).

473 43. Gao, M. *et al.* Expansion Stimulated Emission Depletion Microscopy (ExSTED).
474 *ACS Nano* **12**, 4178–4185 (2018).

475 44. Halpern, A. R., Alas, G. C. M., Chozinski, T. J., Paredez, A. R. & Vaughan, J. C.
476 Hybrid Structured Illumination Expansion Microscopy Reveals Microbial
477 Cytoskeleton Organization. *ACS Nano* **11**, 12677–12686 (2017).

478 45. Mahecic, D., Testa, I., Griffié, J. & Manley, S. Strategies for increasing the
479 throughput of super-resolution microscopies. *Curr. Opin. Chem. Biol.* **51**, 84–91
480 (2019).

481

482

483 **Figures and captions:**

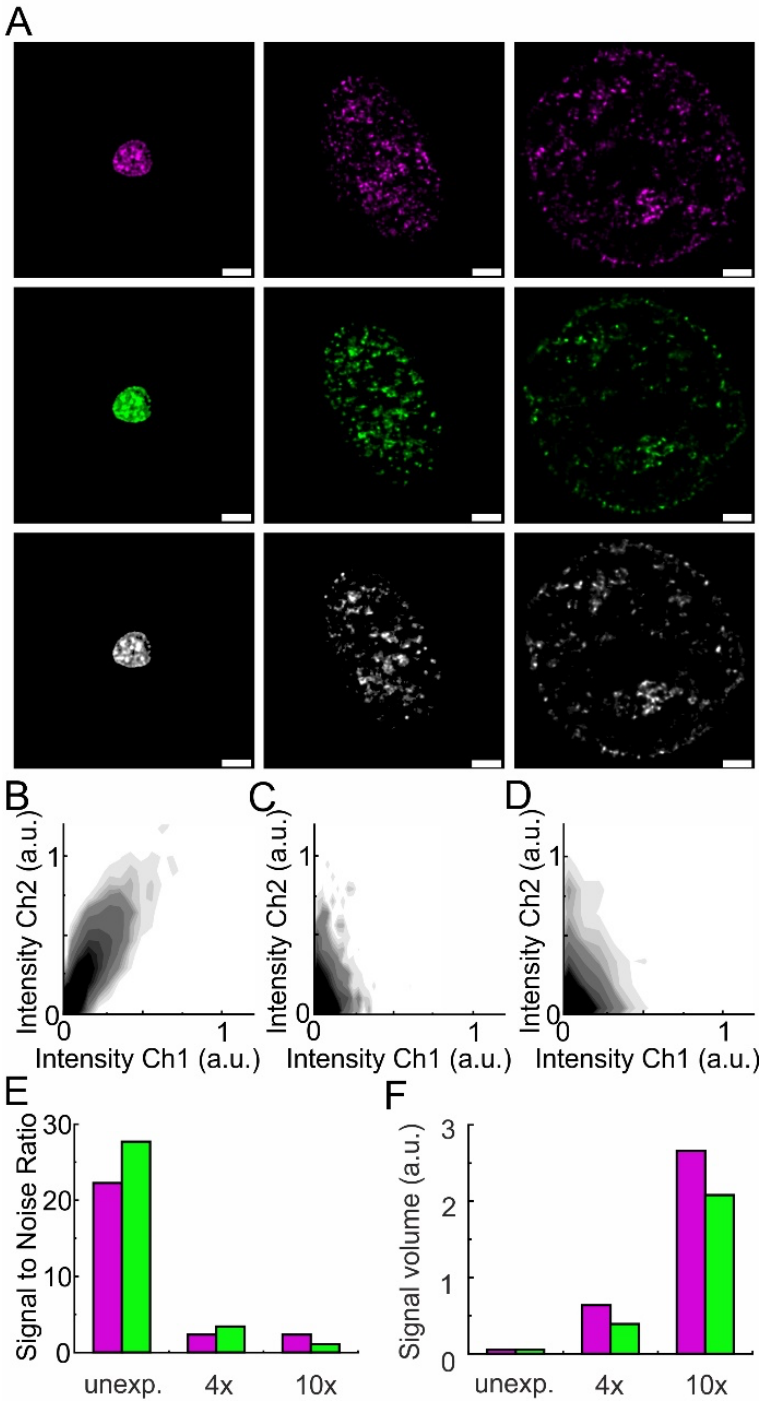

Figure 1. Colocalization analysis of receptor distributions on expanded platelets. A, Deconvolved confocal image planes of the GPIIb/IIIa receptor distribution in unexpanded (left panels), 4x expanded (middle panels) and 10x expanded (right panels) resting platelets immunolabeled with the monoclonal antibody MWReg30 (magenta:

Alexa Fluor 594, green: Alexa Fluor 488, white: merged). **B-D,** Density plots of the signal intensities in channel 1 (Ch1, MWReg30-Alexa Fluor 594) and channel 2 (Ch2, MWReg30-Alexa Fluor 488) in logarithmic scale **(B)** unexpanded, **(C)** 4x expanded and **(D)** 10x expanded. **(E-F)** Signal to noise ratio **(E)** and signal volume **(F)** of the respective color channels derived from raw images in **(A)**. Scale bars 3 µm.

484

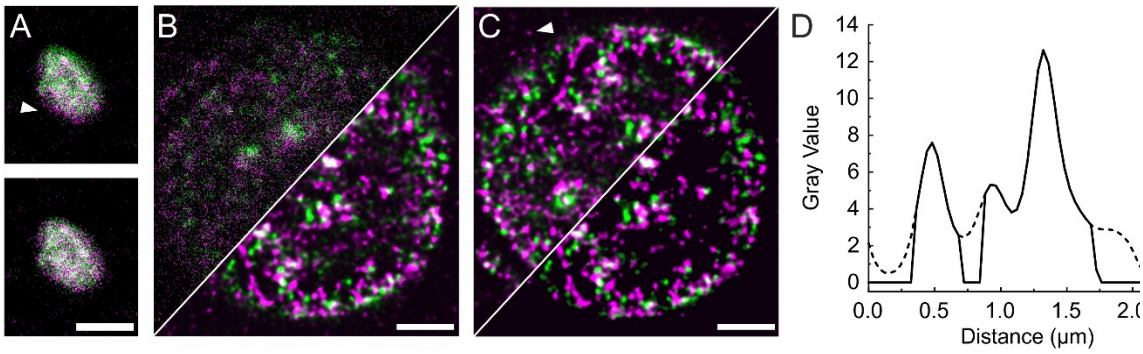

Figure 2. Image preprocessing.

Prior to the colocalization analysis confocal z-stacks of GPIIb/IIIa receptor distributions (MWReg30; green: Alexa Fluor 488, magenta: Alexa Fluor 594) are processed by **(A)** a chromatic shift correction: raw unexpanded platelet, **(B)** image deconvolution: raw (left) and deconvolved (right) image of 4x expanded platelet, **(C)** masking the surface: deconvolved (left) and masked surface (right) of 4x expanded platelet. **(D)** Line plots of signal intensity before (dashed line) and after creating a masked surface (solid line) derived from images in **(C)**. Scale bars 3µm.

485

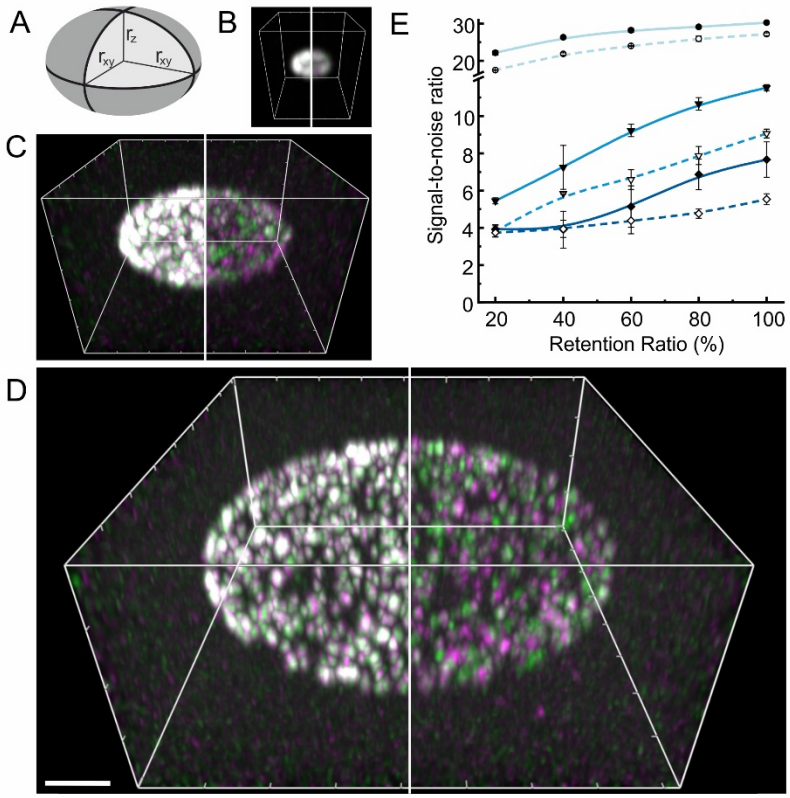

Figure 3. Simulated platelet receptor distributions.

A, Randomly distributed single GPIIb/IIIa receptors or receptor clusters positions were placed on a spheroid surface reflecting typical mouse platelet dimensions (r_{xy} = 1.5 µm and r_z = 0.5 µm). **B-D,** Based on the simulated receptor distributions and the antibody and marker combination (Case I: left, Case II: right) realistic 3D fluorescence images were created including the generation of background signal and noise for **B** unexpanded, **C** 4x expanded (brightness increased 2x) and **D** 10x expanded platelets (brightness increased 10x). In the images presented here the marker retention ratio is 100%. **E,** Signal-to-noise ratio of simulated 3D images in Case I (solid lines, filled symbols) and Case II (dashed lines, open symbols) of unexpanded (light blue), 4x expanded (medium blue) and 10x expanded platelets for a marker retention ratio ranging from 20% to 100%. Scale bar B-D 4 µm

486

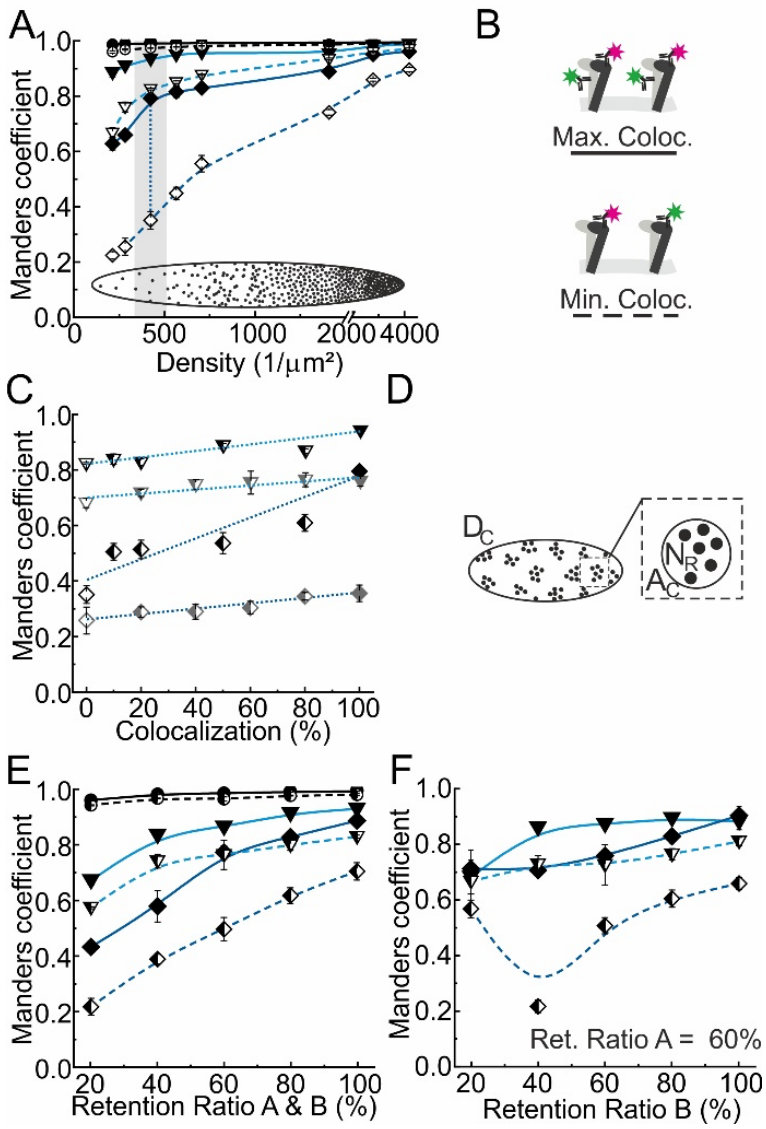

Figure 4. Investigating the influence of receptor densities and label retention ratios of the accuracy and resolution of colocalization analysis with ExM based on simulated receptor distributions.

A, Density dependence of the Manders' coefficients for the maximum (solid lines & filled symbols) and minimum (dashed lines & open symbols) colocalization cases illustrated in (B); non-interacting receptor distributions on unexpanded (black), 4x expanded (light blue) and 10x expanded platelets (dark blue) with corresponding SD (error bars). The lines show the trend with a B-spline, the gray shaded area highlights the expected range of the average density of GPIIb/IIIa receptors and the dotted line indicates the dynamic range of the Manders' coefficient. **B,** Cartoon of the maximum and minimum colocalization test case. **C,** Manders' coefficients with

corresponding SD (error bars) of simulated receptor distributions with different degrees of colocalization on 4x (triangles) and 10x (diamonds) expanded platelets for a label retention ratio of 100% (black symbols) and 50 % (gray symbols) with a linear fit (dotted lines) at the receptor density expected for GPIIb/IIIa (dotted line in in A). **D,** Cartoon of a clustered receptor distribution indicating the cluster density D_C, cluster area A_C and the number of receptors per cluster N_R (for GPIIb/IIIa: D_C=70 μm^{-1}, A_C=300 nm and N_R=7, see supplemental Figure III). **E,F** Manders' coefficients with corresponding SD (error bars) in simulated receptor cluster distributions for the maximum (solid lines, filled symbols) and minimum (dashed lines, half-filled symbols) colocalization test cases in the case of **(E)** equal and **(F)** asymmetric scenarios of label retention, unexpanded (black), 4x expanded (light blue) and 10x expanded platelets (dark blue).

487

488

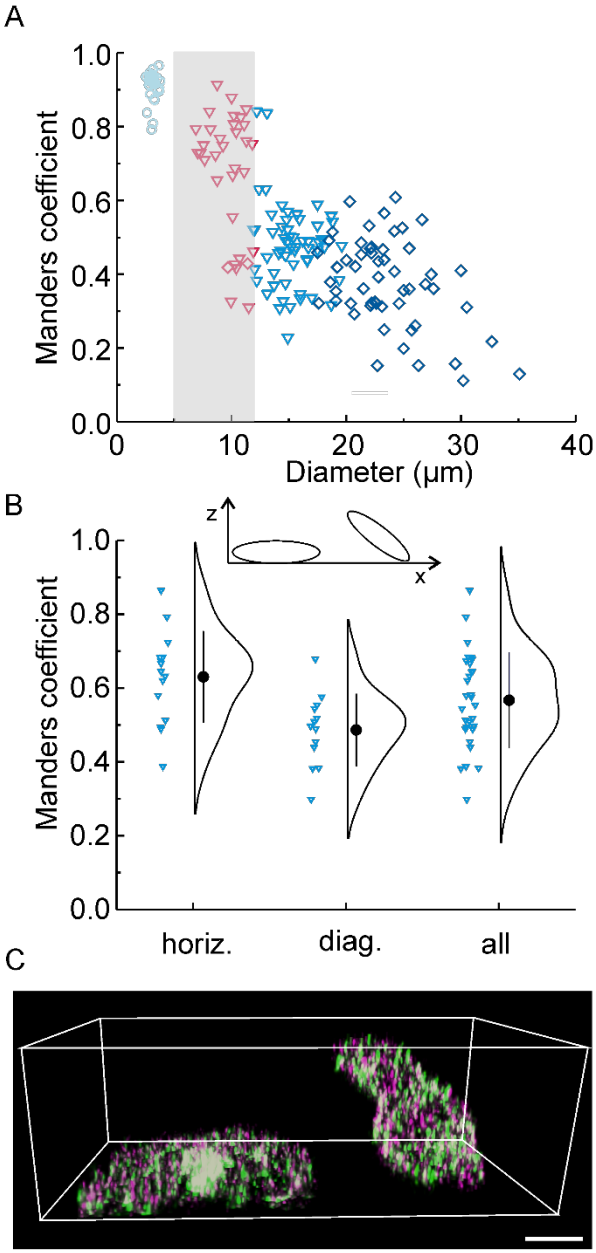

Figure 5. Manders' colocalization coefficient dependence on expansion factor and orientation.

A, Manders' colocalization coefficient vs. diameter of unexpanded (circles), 4x expanded (triangles) and 10x expanded (diamonds) resting platelets labeled with anti-GPIIb/IIIa antibodies (MWReg30) carrying Alexa Fluor 488 and anti-GPIX antibodies (p0p6) carrying Alexa Fluor 594 (Case III). Expanded platelets with a diameter below 12 µm were excluded from further analysis (marked in red) (**B-C**) **B,** Distributions of the

Manders' colocalization coefficients of 4x expanded resting platelets labeled with an anti-GPIIb/IIIa antibody (MWReg30) carrying either Alexa Fluor 488 (green in C) or Alexa Fluor 594 (magenta in C, Case II) selected for horizontal (horiz.) or diagonal (diag.) orientation and without any selection (all).**C,** Two example platelets from the data in B exhibiting horizontal (left) and diagonal (right) orientation. Scale bar 4 µm

489

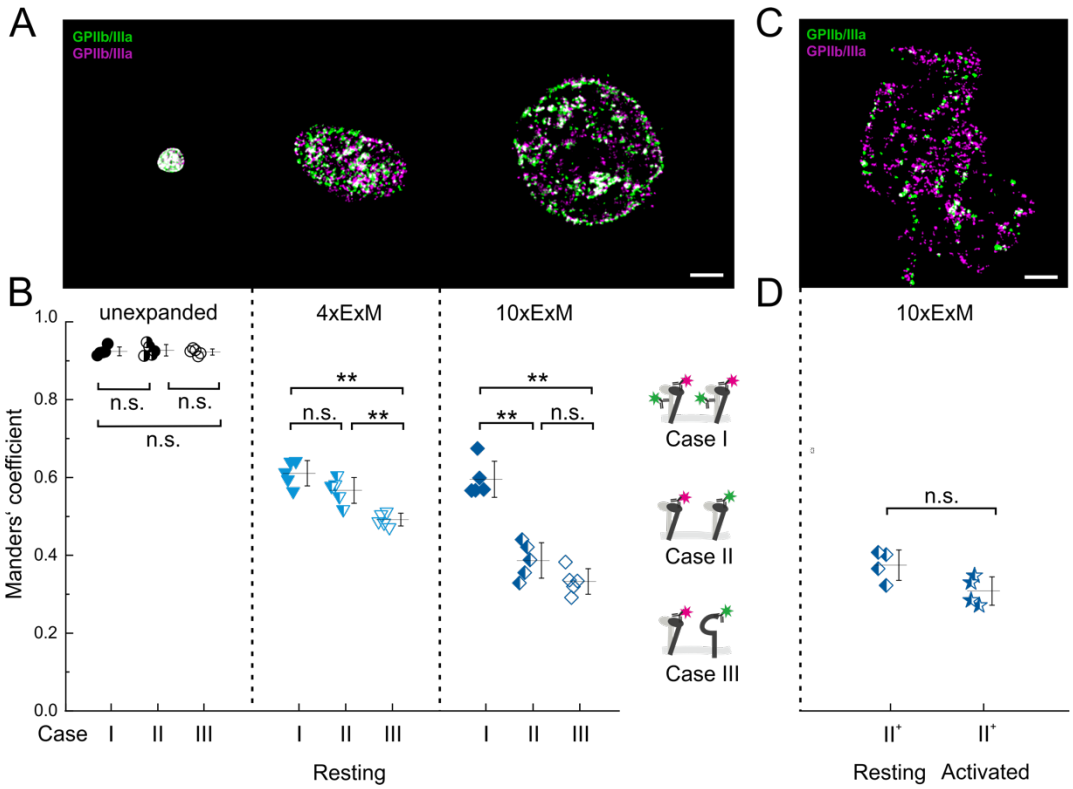

Figure 6. Performance of ExM based colocalization analysis.

A, Deconvolved confocal image slices of GPIIb/IIIa receptors on unexpanded (left), 4x expanded (middle) and 10x expanded (right) resting platelets,all directly labeled with fluorescent antibodies (Alexa Fluor 488 (green) or Alexa Fluor 594 (magenta). **B,** Comparing the distributions of the average Manders' coefficients of groups of six with corresponding SD (error bars) of unexpanded (left, black circles), 4x expanded (middle, light blue triangles) and 10x expanded (right, dark blue diamonds) resting platelets labeled with three different combinations of antibodies (Case I: filled symbols, Case II: half-filled symbols & Case III: open symbols). **C,** Deconvolved confocal image slice of GPIIb/IIIa receptors on a 10x expanded activated platelet, directly labeled with fluorescent antibodies (Alexa Fluor 488 (green) or Alexa Fluor 594 (magenta).**D,** Distributions of the average Manders' coefficients of groups of five with corresponding SD (error bars) of 10x expanded resting (dark blue diamonds) and activated platelets (dark blue stars) with labeling scheme Case II^+ (Antibody batch 2 with lower density of labeling, see supplemental Table I). n.s.: $p > 0.05$, *: $p \leq 0.05$, **: $p \leq 0.01$, (Kruskal-Wallis ANOVA test), scale bars 5 µm.

490